

Ionospheric Effects on Microwave Signals

Mahdi M. Alizadeh, Dudy D. Wijaya, Thomas Hobiger,
Robert Weber and Harald Schuh

Abstract The ionosphere is a dispersive medium for space geodetic techniques operating in the microwave band. Thus, signals traveling through this medium are—to the first approximation—affected proportionally to the inverse of the square of their frequencies. This effect, on the other hand, can reveal information about the parameters of the ionosphere in terms of Total Electron Content (TEC) of the electron density. This part of the book provides an overview of ionospheric effects on microwave signals. First, the group and phase velocities are defined along with the refractive index in the ionosphere and the ionospheric delay. Then, we focus mainly on the mitigation and elimination of ionospheric delays in the analysis of space

M. Mahdi Alizadeh (✉)

Department for Geodesy and Geoinformation Science, Technical University of Berlin,
Strasse des 17. Juni, 135, 10623 Berlin, Germany
e-mail: mahdi.alizadeh@mail.tu-berlin.de

D. D. Wijaya

Geodesy Research Group, Institute of Technology Bandung,
Ganesha 10, Bandung-West Java, Indonesia
e-mail: dudy@gd.itb.ac.id

T. Hobiger

Space-Time Standards Laboratory, Applied Electromagnetic Research,
National Institute of Information and Communications Technology,
4-2-1 Nukui-Kitamachi, Koganei, 184-8795 Tokyo, Japan
e-mail: hobiger@nict.go.jp

R. Weber

Department of Geodesy and Geoinformation, Vienna University of Technology,
Gußhausstraße 27-29, 1040 Vienna, Austria
e-mail: robert.weber@tuwien.ac.at

H. Schuh

Department 1 Geodesy and Remote Sensing,
Helmholtz Centre Potsdam GFZ German Research Centre for Geosciences,
Telegrafenberg A 17, 14473 Potsdam, Germany
e-mail: schuh@gfz-potsdam.de

geodetic observations, specifically for Global Navigation Satellite Systems (GNSS) and Very Long Baseline Interferometry (VLBI) observations. In particular, we summarize existing models as well as strategies based on observations at two or more frequencies to eliminate first and higher order delays. Finally, we review various space geodetic techniques (including satellite altimetry and radio occultation data) for estimating values and maps of TEC.

1 Group and Phase Velocity

The characteristic of an electromagnetic wave propagating in space is defined by its frequency f and wavelength λ . In a dispersive medium, the propagation velocity of an electromagnetic wave is dependent on its frequency. In such a medium the propagation velocities of a sinusoidal wave and a wave group are different. The propagation velocity of a sinusoidal wave with a uniform wavelength is called the phase velocity v_{ph} , while the propagation velocity of the wave group is referred to as group velocity v_{gr} . Within the vacuum the phase and group velocities are the same, but in the real conditions, this is not the case. Following Wells (1974) the velocity of phase is

$$v_{ph} = \lambda f. \quad (1)$$

In general, the carrier waves propagate with the phase velocity. For the group velocity we have (Hofmann-Wellenhof et al. 1993)

$$v_{gr} = - \left(\frac{df}{d\lambda} \right) \lambda^2. \quad (2)$$

According to Bauer (2003) for Global Navigation Satellite Systems (GNSS), modulated code signals propagate with the group velocity.

By forming the differential of Eq. 1 we get

$$dv_{ph} = f d\lambda + \lambda df. \quad (3)$$

This equation can be re-arranged to

$$\frac{df}{d\lambda} = \frac{1}{\lambda} \frac{dv_{ph}}{d\lambda} - \frac{f}{\lambda}. \quad (4)$$

Substituting Eq. 4 into Eq. 2 yields the relation between group and phase velocities

$$v_{gr} = v_{ph} - \lambda \frac{dv_{ph}}{d\lambda}. \quad (5)$$

In a non-dispersive media phase and group velocities are the same and are equal or lower than the speed of light $c = 299792458 \text{ ms}^{-1}$ in vacuum.

As we know the wave propagation velocity in a medium depends on the refractive index n of that medium. So in principle we have

$$v = \frac{c}{n}. \quad (6)$$

Implementing this equation to the phase and group velocities, the formulae for the phase and group refractive indices n_{ph} and n_{gr} read

$$v_{ph} = \frac{c}{n_{ph}}, \quad (7)$$

$$v_{gr} = \frac{c}{n_{gr}}. \quad (8)$$

Differentiating Eq. 7 with respect to λ yields

$$\frac{dv_{ph}}{d\lambda} = -\frac{c}{n_{ph}^2} \frac{dn_{ph}}{d\lambda}. \quad (9)$$

Substituting Eqs. 9, 8, and 7 into Eq. 5 yields

$$\frac{c}{n_{gr}} = \frac{c}{n_{gr}} + \lambda \frac{c}{n_{ph}^2} \frac{dn_{ph}}{d\lambda}, \quad (10)$$

or

$$\frac{1}{n_{gr}} = \frac{1}{n_{ph}} \left(1 + \lambda \frac{1}{n_{ph}} \frac{dn_{ph}}{d\lambda} \right). \quad (11)$$

Using the approximation $(1 + \varepsilon)^{-1} \doteq 1 - \varepsilon$, valid for small quantities of ε , Eq. 11 is inverted to

$$n_{gr} = n_{ph} \left(1 - \lambda \frac{1}{n_{ph}} \frac{dn_{ph}}{d\lambda} \right). \quad (12)$$

Thus the group refractive index follows

$$n_{gr} = n_{ph} - \lambda \frac{dn_{ph}}{d\lambda}, \quad (13)$$

Equation 13 is the modified Rayleigh equation (Hofmann-Wellenhof et al. 1993). A slightly different form is obtained by differentiating the relation $c = \lambda f$ with respect to λ and f , that is

$$\frac{d\lambda}{\lambda} = -\frac{df}{f}, \quad (14)$$

and by substituting the results into Eq. 13, the group refractive index yields

$$n_{gr} = n_{ph} + f \frac{dn_{ph}}{df}. \quad (15)$$

2 Ionosphere Refractive Index

The ionosphere is a dispersive medium with respect to microwave signals. This means that the propagation of microwave signals through the ionosphere depends on the frequency of the signals. In order to quantify these effects, the refractive index of the ionosphere must be specified. For a general derivation of the refractive index n in the ionosphere, we refer to Budden (1985). If the collision effects of the particles are ignored, the formula for the phase ionospheric refractive index can be presented as

$$n_{ph}^2 = 1 - \frac{X}{1 - \frac{\frac{1}{2}Y^2 \sin^2 \theta}{1-X} \pm \frac{1}{1-X} \left(\frac{1}{4}Y^4 \sin^4 \theta + Y^2 \cos^2 \theta (1-X)^2 \right)^{1/2}}, \quad (16)$$

where

$$X = \frac{\omega_0^2}{\omega^2}, \quad Y = \frac{\omega_H}{\omega},$$

$$\omega_0 = 2\pi f_0 = \sqrt{\frac{N_e e^2}{\epsilon_0 m_e}}, \quad \omega_H = 2\pi f_H = \frac{B_0 |e|}{m_e},$$

n	complex refractive index	N_e	electron density
$\omega = 2\pi f$	(radial frequency)	f	wave frequency
ω_0	electron plasma frequency	ω_H	electron gyro frequency
ϵ_0	permittivity of free space	B_0	magnitude of the magnetic field vector \mathbf{B}_0
θ	angle between the ambient magnetic field vector and the wave vector	e	electron charge
		m_e	electron mass

Equation 16 is called the Appleton-Hertree formula for the ionospheric refractive index of phase. To evaluate the ionospheric effects more easily, various approximations of Eq. 16 were proposed. According to Tucker and Fanin (1968) and Hartmann and Leitinger (1984) the traditional way of deriving approximate expressions of the refractive index is by assuming that the magnetic field is associated with the propagation direction, with $\sin \theta \approx 0$. Without taking any assumptions about the propagation direction, Brunner and Gu (1991) preferred to use the order of magnitude of the various terms in Eq. 16 in deriving a suitable approximate expression for the ionospheric refractive index and their result is identical to the quasi-longitudinal refractive index expression derived by Budden (1985).

$$n_{ph}^{ion} = 1 - \frac{X}{2} \pm \frac{XY}{2} \cos \theta - \frac{X^2}{8}. \quad (17)$$

Following Brunner and Gu (1991), it is convenient to define the constants C_X and C_Y as

$$C_X \equiv \frac{e^2}{4\pi^2 \epsilon_0 m_e} = 80.62, \quad (18)$$

$$C_Y \equiv \frac{\mu_0 e}{2\pi m_e}, \quad (19)$$

so that Eq. 17 can be expressed in orders of $\frac{1}{f^n}$

$$n_{ph}^{ion} = 1 - \frac{C_X}{2} N_e f^{-2} \pm \frac{C_X C_Y}{2} N_e B_0 \cos \theta f^{-3} - \frac{C_X^2}{8} N_e^2 f^{-4}, \quad (20)$$

where N_e is the electron density and μ_0 is the permeability in vacuum.

Equation 20 includes the first-order term and higher order terms of the ionospheric propagation effects on microwave frequencies.

First Order Refractive Index

The first two terms in Eq. 20 are denoted as the first order refractive index. Since the third- and fourth-order terms are orders of magnitude smaller than the second-order term, they are in first approximation usually neglected (Alizadeh et al. 2011). Thus, Eq. 20 can be reduced to

$$n^{ion} = 1 - \frac{C_X}{2} N_e f^{-2}. \quad (21)$$

Evaluating the constant factor in Eq. 21, we obtain:

$$C_2 = \frac{C_X}{2} = \frac{e^2}{8\pi^2 \epsilon_0 m_e} \approx 40.31 \text{ [m}^3/\text{s}^2\text{]}. \quad (22)$$

By substituting Eq. 22 into Eq. 21 the first-order refractive index is obtained. Equation 21 is used for the phase measurements, so it is denoted as phase refractive index n_{ph}^{ion} :

$$n_{ph}^{ion} = 1 - C_2 \frac{N_e}{f^2} = 1 - 40.31 \frac{N_e}{f^2}. \quad (23)$$

In order to obtain the group refractive index, Eq. 23 is differentiated:

$$\frac{dn_{ph}}{df} = \frac{2C_2}{f^3} N_e, \quad (24)$$

substituting Eqs. 23 and 24 into Eq. 15 yields:

$$n_{gr}^{ion} = 1 - \frac{C_2}{f^2} N_e + f \frac{2C_2}{f^3} N_e df, \quad (25)$$

or

$$n_{gr}^{ion} = 1 + C_2 \frac{N_e}{f^2} = 1 + 40.31 \frac{N_e}{f^2}. \quad (26)$$

It can be seen from Eqs. 23 and 26 that the group and phase refractive indices have the same diversity from one but with an opposite signs. As $n_{gr} > n_{ph}$ it is simply concluded that $v_{gr} < v_{ph}$. As a consequence of the different velocities, when a signal travels through the ionosphere, the carrier phase is advanced and the modulated code is delayed. In the case of GNSS, code measurements which propagate with the group velocity are delayed and the phase measurements that propagate with phase velocity are advanced. Therefore, compared to the geometric distance between a satellite and a receiver, the code pseudo-ranges are measured too long and phase pseudo-ranges are measured too short. The amount of this difference is in both cases the same (Hofmann-Wellenhof et al. 1993).

High Order Refractive Index

The first order refractive index only accounts for the electron density within the ionosphere, while the effect of the Earth's magnetic field and its interactions with the ionosphere are considered in the higher order terms; i.e. the third and fourth terms of Eq. 20. For precise satellite positioning, these terms have to be considered as they will introduce an ionospheric delay error of up to a few centimeters (Brunner and Gu 1991; Bassiri and Hajj 1993).

3 Ionospheric Delay

According to Fermat's principle (Born and Wolf 1964), the measured range s is defined by

$$s = \int n ds, \quad (27)$$

where the integration is performed along the path of the signal. The geometric distance s_0 between the satellite and the receiver may be obtained analogously by setting $n = 1$:

$$s_0 = \int ds_0. \quad (28)$$

The delay (or advance) experienced by signals traveling through the ionosphere is the difference between measured and geometric range. This is called the ionosphere delay or ionospheric refraction:

$$\Delta\rho^{ion} = \int n ds - \int ds_0. \quad (29)$$

By substituting Eq. 20 into Eq. 29, the ionospheric total delay for the phase observations is expressed as

$$\Delta\rho_{ph}^{ion} = -\frac{C_X}{2f^2} \int N_e ds \pm \frac{C_X C_Y}{2f^3} \int N_e B_0 \cos \theta ds - \frac{C_X^2}{8f^4} \int N_e^2 ds + \kappa, \quad (30)$$

where $\kappa = \int ds - \int ds_0$ represents the curvature effect. The first three-terms of Eq. 30 denote the first order and higher order ionospheric delays. Assuming that the integrations are evaluated along the geometric path s_0 for simplification, the curvature effect is neglected; thus ds turns to ds_0 and the equation results in

$$\Delta\rho_{ph}^{ion} = -\frac{C_X}{2f^2} \int N_e ds_0 \pm \frac{C_X C_Y}{2f^3} \int N_e B_0 \cos \theta ds_0 - \frac{C_X^2}{8f^4} \int N_e^2 ds_0. \quad (31)$$

First Order Delay

In the first-order approximation, the ionospheric delay for phase measurements is derived by neglecting the second and third terms of Eq. 31 and making use of Eq. 22:

$$\Delta\rho_{ph}^{ion1} = -\frac{C_2}{f^2} \int N_e ds_0, \quad (32)$$

by substituting C_2 from Eq. 22 we get the phase delay

$$\Delta\rho_{ph}^{ion1} = -\frac{40.31}{f^2} \int N_e ds_0. \quad (33)$$

The group delay is similarly obtained using Eq. 26

$$\Delta\rho_{gr}^{ion1} = \frac{40.31}{f^2} \int N_e ds_0. \quad (34)$$

Second Order Delay

According to Eq. 31, the second order ionospheric phase delay is

$$\Delta\rho_{ph}^{ion2} = \frac{C_X C_Y}{2f^3} \int N_e B_0 \cos \theta ds_0. \quad (35)$$

Examining the constants C_X and C_Y , Eq. 35 can be written as

$$\Delta\rho_{ph}^{ion2} = -\frac{7527 c}{2f^3} \int N_e B_0 \cos \theta ds_0, \quad (36)$$

where c is the speed of light. In order to solve Eq. 36, information of the magnetic field B_0 and the angle θ along the ray path have to be known. Since this is difficult to accomplish, Brunner and Gu (1991) assumed that $B_0 \cos \theta$ does not vary greatly along the ray path, so that one may take the average $\overline{B_0 \cos \theta}$ in front of the integration:

$$\Delta\rho_{ph}^{ion2} = -\frac{7527 c}{2f^3} \overline{B_0 \cos \theta} \int N_e ds_0. \quad (37)$$

An alternative way was proposed by Bassiri and Hajj (1993) who assumed the Earth's magnetic field as a co-centric tilted magnetic dipole and approximated the ionospheric layer as a thin shell at the height of 400km. Thus, the magnetic field vector \mathbf{B}_0 can be written as:

$$\mathbf{B}_0 = B_g \left(\frac{R_E}{R_E + H} \right) [\sin \theta_m \cdot \mathbf{Y}_m - 2 \cos \theta_m \cdot \mathbf{Z}_m], \quad (38)$$

B_g represents the magnitude of the magnetic field near the equator at surface height ($B_g \approx 3.12 \times 10^{-5}$ T). R_E is the Earth's radius ($R_E \approx 6,370$ km). H denotes the height of the ionospheric thin shell above the Earth's surface ($H = 400$ km). \mathbf{Y}_m and \mathbf{Z}_m are the Y and Z unit vectors in the geomagnetic coordinate system, and θ_m is the angle between the ambient magnetic field vector and wave vector in the geomagnetic coordinate system (see Sect. 4.3). The scalar product of the magnitude field vector B_0 and the signal propagation unit vector \mathbf{k} is:

$$\mathbf{B}_0 \cdot \mathbf{k} = B_0 |\mathbf{k}| \cos \theta = B_0 \cos \theta. \quad (39)$$

Combining Eqs. 36, 38, and 39, an expression similar to Eq. 37 can be derived

$$\Delta\rho_{ph}^{ion2} = -\frac{7527 c}{2f^3} \mathbf{B}_0 \cdot \mathbf{k} \int N_e ds_0. \quad (40)$$

Equation 40 is sufficient to approximate the effect of the second order term to better than 90 % on the average (Fritsche et al. 2005).

Third Order Delay

According to Eq. 31 and evaluating the constant C_X , the third order ionospheric phase delay is expressed as

$$\Delta\rho_{ph}^{ion3} = -\frac{812.4}{f^4} \int N_e^2 ds_0. \quad (41)$$

Brunner and Gu (1991) applied the shape parameter η in such a way that the integral in Eq. 41 can be approximated by

$$\int N_e^2 ds_0 = N_{max} \eta \int N_e ds_0. \quad (42)$$

The shape parameter η may be assumed with 0.66 as an appropriate value to account for different electron density distributions. N_{max} represents the peak electron density along the ray path. Substituting Eq. 42 into Eq. 41, the third order ionospheric phase delay can be written as:

$$\Delta\rho_{ph}^{ion3} = -\frac{812.4}{f^4} N_{max} \eta \int N_e ds_0. \quad (43)$$

Integrated Electron Density

As already shown, the first, second and third order ionospheric delays require the distribution of the electron density N_e along the ray path. If one is interested in signal propagation in the ionosphere, however, the integral of the electron density along the ray path becomes relevant (e.g. Schaer 1999). This quantity is defined as the Total Electron Content (TEC) and represents the total amount of free electrons in a cylinder with a cross section of 1 m^2 and a height equal to the slant signal path. TEC is measured in Total Electron Content Unit (TECU), with 1 TECU equivalent to 10^{16} electrons/ m^2 . For an arbitrary ray path the slant TEC (STEC) can be obtained from

$$STEC = \int N_e(s) ds, \quad (44)$$

where N_e is the electron density along the line of sight ds .

Using Eq. 44 the relation between the total electron content in TECU and ionospheric delay in meters can be obtained. Taking Eq. 33 into account for the carrier phase measurements we get

$$\Delta\rho_{ph}^{ion} = -\frac{40.31}{f^2} STEC \quad [\text{m}], \quad (45)$$

in the case of group delay measurements, the result is the same, but with opposite sign

$$\Delta\rho_{gr}^{ion} = \frac{40.31}{f^2} STEC \quad [\text{m}]. \quad (46)$$

Finally, using the constant derived from Eq. 22 the factor ϑ can be defined as the ionospheric path delay in meters per one TECU, related to a certain frequency f in Hz

$$\vartheta = \frac{40.31 \cdot 10^{16}}{f^2} \quad [\text{m}/\text{TECU}]. \quad (47)$$

Table 1 Relation between various GPS first-order measured parameters and TEC of Earth's ionosphere extracted from Klobuchar (1996)

$L_2 - L_1$, differential group delay caused by the ionosphere	
1 ns of differential code delay	2.852×10^{16} el/m ² 1.546 ns of delay at L_1 0.464 m of range error at L_1
1 ns of delay, measured at L_1	1.8476×10^{16} el/m ² 0.300 m of range error at L_1
1 m of range error	Measured at $L_1 = 6.15 \times 10^{16}$ el/m ² Measured at $L_2 = 3.73 \times 10^{16}$ el/m ²
1 TEC units [1×10^{16} el/m ²]	0.351 ns of differential delay 0.524 ns of delay at L_1 0.163 m of range delay at L_1 0.853 cycles of phase advance at L_1

Table 1 shows some relations between the various GPS parameters and the TEC extracted from Klobuchar (1996).

Single Layer Model and Mapping Function

For absolute TEC mapping using ground-based GNSS data, TEC along the vertical should be taken into account. Since GPS basically provides measurements of STEC, an elevation dependent mapping function is required which describes the ratio between the STEC and the vertical TEC (VTEC):

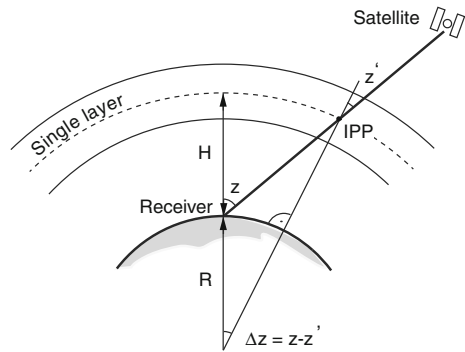
$$F(z) = \frac{STEC}{VTEC}. \quad (48)$$

To get an approximation, a single-layer model (SLM) is usually adopted for the ionosphere. In SLM it is assumed that all free electrons are concentrated in an infinitesimally thin layer above the Earth's surface (Schaer 1999). The height H of that shell is usually set between 350 and 500 km, which is slightly above the height where the highest electron density is expected (approximately above the height of the F2 layer peak). Figure 1 depicts the basic geometry of the SLM in the sun-fixed coordinate system. The signal transmitted from the satellite to the receiver crosses the ionospheric shell in the so-called ionospheric pierce point (IPP). The zenith angle at the IPP is z' and the signal arrives at the ground station with zenith angle z . From Fig. 1 the relation between z' and z could be derived:

$$\sin z' = \frac{R}{R + H} \sin z. \quad (49)$$

In Eq. 49 $R \approx 6,370$ km is the mean Earth radius and H is the height of the single layer in km.

Fig. 1 Single-layer model for the ionosphere (modified from Todorova 2008)



Applying Eq. 49 and the TEC definition Eq. 44 in Eq. 48 leads to the so-called SLM mapping function

$$F(z) = \frac{1}{\cos z'} = \frac{1}{\sqrt{1 - \sin^2 z'}}, \tag{50}$$

where z' is obtained from Eq. 49.

A modified single-layer mapping function (MSLM) is adopted by Dach et al. (2007):

$$F(z) \cong \frac{1}{\sqrt{1 - \left(\frac{R}{R+H} \sin(\alpha z)\right)^2}}, \tag{51}$$

where $\alpha = 0.9782$ and $H = 506.7$ km. It should be clarified that the only difference between MSLM and SLM is the heuristic factor α . The MSLM approximates the Jet Propulsion Laboratory (JPL) extended slab model mapping function. Based on results showing that a single layer height of 550 km tends to be the best choice overall, the extended slab model provides an approximation which closely matches a single layer model with the same shell height of 550 km (Sparks et al. 2000).

4 How to Deal with Ionospheric Delay

The most important parameter of the ionosphere that affects the GNSS signals is the total number of electrons within the ionosphere. As already described in Sect. 3 the integrated number of electrons, commonly called TEC, is expressed as the number of free electrons in a column with 1 m^2 cross section, extending from the receiver to the satellite. This can be seen from Eqs. 45 and 46, where the changes in the range caused by the ionospheric refraction were directly related to the determination of TEC. There are different ways to deal with ionosphere and TEC; some methods are discussed in the following:

4.1 Modeling TEC Using Physical and Empirical Models

4.1.1 Klobuchar Model

In the mid-80s, a simple algorithm was developed for the GPS single-frequency users to correct about 50% of the ionospheric range error. This correction method was established because the GPS satellite message had space for only eight coefficients to describe the worldwide behavior of the Earth's ionosphere. Furthermore, these coefficients could not be updated more often than once per day, and generally not even that often. Finally, simple equations had to be used to implement the algorithm to avoid causing excessive computational stress on the GPS users. The algorithm was developed by Klobuchar (1986) and led to the model that approximated the entire ionospheric vertical refraction by modeling the vertical time delay for the code pseudo-ranges.

The Klobuchar model does not directly compute the TEC. Instead, it models time delay due to ionospheric effects. Equation 52 shows time delay in nanoseconds. Multiplying this expression by the speed of light will result the vertical ionospheric range delay. The obtained range delay, after applying the SLM function, can be used to correct the ionospheric error in the measurements. Although the model is an approximation, it is nevertheless of importance because it uses the ionospheric coefficients broadcast within the fourth sub frame of the navigation message (Hofmann-Wellenhof et al. 1993). The time delay derived from the Klobuchar model follows from

$$\Delta T_v^{ion} = A_1 + A_2 \cos\left(\frac{2\pi(t - A_3)}{A_4}\right), \quad (52)$$

with

$$\begin{aligned} A_1 &= 5 \cdot 10^{-9} \text{ s} = 5 \text{ ns}, \\ A_2 &= \alpha_1 + \alpha_2 \varphi_{IP}^m + \alpha_3 \varphi_{IP}^{m^2} + \alpha_4 \varphi_{IP}^{m^3}, \\ A_3 &= 14^h \text{ local time}, \\ A_4 &= \beta_1 + \beta_2 \varphi_{IP}^m + \beta_3 \varphi_{IP}^{m^2} + \beta_4 \varphi_{IP}^{m^3}. \end{aligned}$$

The values A_1 and A_3 are constant values, the coefficients $\alpha_i, \beta_i, i = 1, \dots, 4$ are uploaded daily from the control segment to the satellites and broadcast to the users through the broadcast ephemeris. t is the local time of the *Ionospheric Pierce Point (IPP)*, and is derived from:

$$t = \frac{\lambda_{IP}}{15} + t_{UT}, \quad (53)$$

where λ_{IP} is the longitude of *IPP* in degrees (positive to East) and t_{UT} is the observation epoch in Universal Time. Finally φ_{IP}^m in Eq. 52 is the geomagnetic latitude of *IPP* and is calculated by Lilov 1972:

$$\cos \varphi_{IP}^m = \sin \varphi_{IP} \sin \varphi_P + \cos \varphi_{IP} \cos \varphi_P \cos(\lambda_{IP} - \lambda_P). \quad (54)$$

At present (as of 2012) the coordinates of geomagnetic pole are:

$$\varphi_P = 80.0^\circ\text{N}, \quad \lambda_P = 72.2^\circ\text{W}. \quad (55)$$

For more details refer to Sect. 4.3 (Bohm et al. 2013).

4.1.2 NeQuick Model

The NeQuick ionospheric model developed by the Aeronomy and Radiopropagation Laboratory (ARPL) of the Abdus Salam International Centre for the Theoretical Physics in Trieste (Italy) and the Institute for Geophysics, Astrophysics and Meteorology of the University of Graz (Austria) allows calculation of TEC and electron density profile for any arbitrary path (Nava 2006). The NeQuick model is based on the so-called DGR model introduced by Di Giovanni and Radicella (1990). The original DGR model uses a sum of Epstein layers to analytically construct the electron density distribution within the ionosphere. The general expression for the electron density in an Epstein layer following (Radicella and Nava 2010) is:

$$N_{Epstein}(h, hm, Nm, B) = \frac{4Nm}{\left(1 + \exp\left(\frac{h-hm}{B}\right)\right)^2} \exp\left(\frac{h-hm}{B}\right), \quad (56)$$

where h is the height, hm is the layer peak height, Nm is the electron density and B is the layer's thickness parameter.

Based on the anchor points related to the ionospheric characteristics which are routinely scaled from ionogram data, the analytical functions are constructed. The basic equations that describe the latest NeQuick model (NeQuick 2) are given by Nava et al. (2008):

$$N_{bot}(h) = N_E(h) + N_{F1}(h) + N_{F2}(h), \quad (57)$$

where:

$$\begin{aligned} N_E(h) &= \frac{4Nm * E}{\left(1 + \exp\left(\frac{h-hmE}{B_E} \xi(h)\right)\right)^2} \exp\left(\frac{h-hmE}{B_E} \xi(h)\right), \\ N_{F1}(h) &= \frac{4Nm * F1}{\left(1 + \exp\left(\frac{h-hmF1}{B_1} \xi(h)\right)\right)^2} \exp\left(\frac{h-hmF1}{B_1} \xi(h)\right), \\ N_{F2}(h) &= \frac{4Nm F2}{\left(1 + \exp\left(\frac{h-hmF2}{B_2}\right)\right)^2} \exp\left(\frac{h-hmF2}{B_2}\right). \end{aligned} \quad (58)$$

With

$$\begin{aligned} Nm * E &= NmE - N_{F1}(hmE) - N_{F2}(hmE), \\ Nm * F1 &= NmF1 - N_E(hmF1) - N_{F2}(hmF1), \end{aligned} \quad (59)$$

and

$$\xi(h) = \exp\left(\frac{10}{1 + 1|h - hmF2|}\right). \quad (60)$$

$\xi(h)$ is a function assuring a fadeout of the E and F1 layers in the proximity of the F2 layer peak in order to avoid the second maxima around $hmF2$. The Nm values are obtained from the critical frequencies obtained from the ionograms. The peak height of the F2 layer $hmF2$ is computed from $M(3000)F2$ and the ratio f_oF2/f_oE . The F1 peak height $hmF1$ is modeled in terms of $NmF1$. The geomagnetic dip of the location and the E peak height hmE is fixed at 120 km. The thickness parameter $B2$ of the F2 layer is calculated using the empirical determination of the base point of the F2 layer defined by Mosert de Gonzalez and Radicella (1990) and the thickness parameters corresponding to the F1 and E regions are adjusted numerically (Radicella and Leitinger 2001).

The NeQuick model gives electron density as a function of geographic latitude and longitude, height, solar activity (specified by the sunspot number or by the 10.7 cm solar radio flux), season (month) and time (Universal or local) (Radicella 2009). The Fortran-77 source code of the NeQuick model is available at Radiocommunication Sector website (ITU 2011). The basic inputs of the code are: position, time and solar flux (or sunspot number) and the output is the electron concentration at any given location in space and time. In addition the NeQuick package includes specific routines to evaluate the electron density along any ray-path and the corresponding TEC by numerical integration (Nava 2006). The first version of the model has been used by the European Space Agency (ESA), European Geostationary Navigation Overlay Service (EGNOS) project for assessment analysis and has been adopted for single-frequency positioning applications in the framework of the European Galileo project. It has also been adopted by the International Telecommunication Union, Radiocommunication Sector (ITU-R) as a suitable method for TEC modeling (ITU 2007).

4.1.3 IRI Model

The International Reference Ionosphere (IRI) is the result of an international cooperation sponsored by the Committee on Space Research (COSPAR) and the International Union of Radio Science (URSI). Since first initiated in 1969, IRI is an internationally recognized standard for the specification of plasma parameters in Earth's ionosphere. It describes monthly averages of electron density, electron temperature, ion temperature, ion composition, and several additional parameters in the altitude range from 60 to 1500 km. IRI has been steadily improved with newer data and better modeling

techniques leading to the release of a number of several key editions of the model. The latest version of the IRI model, IRI-2012 (Bilitza et al. 2011), will include significant improvements not only for the representations of electron density, but also for the description of electron temperature and ion composition. These improvements are the result of modeling efforts, since the last major release, IRI-2007 (Bilitza and Reinisch 2007). IRI is an empirical model based on most of the available data sources for the ionospheric plasma. The data sources of IRI include the worldwide network of ionosondes, which is monitoring the ionospheric electron densities at and below the F-peak since more than fifty years, the powerful incoherent scatter radars which measure plasma temperatures, velocities, and densities throughout the ionosphere, at eight selected locations, the topside sounder satellites which provide a global distribution of electron density from the satellite altitude down to the F-peak, in situ satellite measurements of ionospheric parameters along the satellite orbit, and finally rocket observations of the lower ionosphere. Since IRI is an empirical model it has the advantage of being independent from the advances achieved in the theoretical understanding of the processes that shape the ionospheric plasma. Nevertheless such an empirical model has a disadvantage of being strongly dependent on the underlying data base. Therefore regions and time periods not well covered by the data base will result a lower reliability of the model in that area (Bilitza et al. 2011).

The vertical electron density profile within IRI is divided into six sub-regions: the topside, the F2 bottom-side, the F1 layer, the intermediate region, the E region valley, the bottom-side E and D region. The boundaries are defined by characteristic points such as F2, F1, and E peaks. The strong geomagnetic control of the F region processes is taken into account for the analysis of the global electron density behavior (Feltens et al. 2010).

IRI has a wide range of applications. Among these applications, IRI has played an important role in geodetic techniques as well. In several studies IRI has been used as a background ionosphere in order to validate the reliability and accuracy of an approach for obtaining ionospheric parameters from geodetic measurements (e.g. Hernández-Pajares et al. 2002). Another field which IRI has helped geodetic techniques is with interpolating in areas with no or few available GPS measurements (e.g. Orús et al. 2002).

4.1.4 GAIM Model

In 1999 the Multidisciplinary University Research Initiatives (MURI) sponsored by the U.S. Department of Defense developed the Global Assimilative Ionospheric Model (GAIM). The GAIM model is a time-dependent, three-dimensional global assimilation model of the ionosphere and neutral atmosphere (JPL 2011). GAIM uses a physical model for the ionosphere/plasmasphere and for assimilating real-time measurements, it uses the Kalman filter approach. Within GAIM the ion and electron volume densities are solved numerically using the hydrodynamic equations for individual ions. The model is physical-based or first-principles based and includes state of the art optimization techniques providing the capability of assimilating differ-

ent ionospheric measurements. GAIM reconstructs 3-dimensional electron density distribution from the height of 90 km up to the geosynchronous altitude (35,000 km) in a continuous basis (Scherliess et al. 2004).

The optimization techniques which is incorporated into GAIM include the Kalman Filter and four dimensional variational (4DVAR) approaches. Currently different data types are being examined with GAIM, these data types include line of sight TEC measurements made from ground-based GPS receiver networks and space-borne GPS receivers, ionosondes, and satellite UV limb scans. To validate the model, different independent data sources were used. These sources are namely VTEC measurements from satellite ocean altimeter radar (such as those onboard TOPEX and Jason-1), ionosonde and incoherent scatter radars (JPL 2011). An updated version of the GAIM model became operational at the Air Force Weather Agency (AFWA) on February, 2008. The new version of GAIM assimilates ultraviolet (UV) observations from Defense Meteorological Satellite Program (DMSP) sensors, including the Special Sensor Ultraviolet Limb Imager (SSULI), which has been developed by the U.S. Naval Research Laboratory (NRL) Space Science Division (NRL 2008).

4.1.5 MIDAS Model

The Multi-Instrument Data Analysis System (MIDAS) was designed and developed at the University of Bath in 2001. The analysis algorithm makes use of GPS dual-frequency observations to produce four-dimensional images of electron concentration over large geographical regions or even over the globe (Mitchell and Cannon 2002). Different types of measurements that can be put into the MIDAS are the satellite to ground measurements, satellite to satellite observations, measurements from sea-reflecting radars, electron-concentration profiles from inverted ionograms, and in-situ measurements of ionized concentration from LEO satellites. The MIDAS algorithm reconstructs the free electron density as a piecewise constant 3D distribution, starting from collections of slant TEC data along ray paths crossing the region of interest (Mitchell and Spencer 2003). The essential ingredient of the MIDAS inversion is the use of Empirical Orthogonal Functions (Sirovich and Everson 1992), along which the solution of the inverse problem is assumed to be linearly decomposable (Materassi 2003). MIDAS produces four-dimensional electron density maps which can be used to correct the phase distortions and polarization changes by Faraday rotation in the ionosphere. MIDAS also has a ray tracer which allows accurate determination of the refracting ray paths and hence the apparent sky location of a radio source.

4.2 Eliminating TEC

TEC is a very complicated quantity. It depends on many parameters such as sunspot activity, seasonal and diurnal variations, the line of signal propagation, and the posi-

tion of the observation site. Therefore it's usually hard to find an appropriate model for it. Thus the most efficient method is to eliminate its effect by using signals in different frequencies. This is the main reason why almost all space geodetic techniques transmit signals in at least two different frequencies. Forming linear combinations with different frequencies allows eliminating the effect of the ionosphere to a large extent.

4.2.1 Eliminating First Order Ionospheric Effects in GNSS Measurements

The fundamental observation equation for the GNSS code-pseudorange including the frequency dependent ionospheric refraction, reads

$$\begin{aligned} P_1 &= \rho + c(\delta t_R - \delta t^S) + \Delta\rho^{trop} + \Delta\rho_{L_1}^{ion} + c(b_R + b^S)_{L_1} + \varepsilon, \\ P_2 &= \rho + c(\delta t_R - \delta t^S) + \Delta\rho^{trop} + \Delta\rho_{L_2}^{ion} + c(b_R + b^S)_{L_2} + \varepsilon, \end{aligned} \quad (61)$$

where

- ρ geometric distance between receiver and satellite
- $\delta t_R, \delta t^S$ receiver and satellite clock offsets to the GPS time
- $\Delta\rho^{trop}$ delay of the signal due to the troposphere
- $\Delta\rho^{ion}$ frequency-dependent delay of the signal due to the ionosphere
- b_R, b^S frequency-dependent hardware delays of the satellite and receiver (DCB) (in ns)
- ε random error

Further corrections like relativistic effects, phase-wind up, or antenna phase center corrections are omitted in Eq. 61.

The code ranges are obtained from measurements of the signals P_1 and P_2 modulated at the two carriers with the frequencies denoted by L_1 and L_2 and the ionospheric term $\Delta\rho^{ion}$ is equivalent to the group delay in Eq. 46.

A linear combination is now performed by

$$P_{1,2} = n_1 P_1 + n_2 P_2, \quad (62)$$

where n_1 and n_2 are factors to be determined in such a way that the ionospheric refraction cancels out. Substituting Eq. 61 into Eq. 62 leads to the postulate

$$n_1 \Delta\rho_{L_1}^{ion} + n_2 \Delta\rho_{L_2}^{ion} = 0. \quad (63)$$

Assuming n_1 and n_2 as

$$n_1 = +\frac{f_{L_1}^2}{f_{L_1}^2 - f_{L_2}^2}, \quad n_2 = -\frac{f_{L_2}^2}{f_{L_1}^2 - f_{L_2}^2}. \quad (64)$$

Substituting these values for n_1 and n_2 , Eq. 63 is fulfilled and the linear combination Eq. 62 becomes:

$$P_{1,2} = \frac{f_{L_1}^2}{f_{L_1}^2 - f_{L_2}^2} P_1 - \frac{f_{L_2}^2}{f_{L_1}^2 - f_{L_2}^2} P_2 = P_3. \quad (65)$$

This is the P_3 ionospheric-free linear combination for code ranges. This linear combination can be written in a more convenient expression:

$$P_3 = \frac{1}{1 - \gamma} (P_1 - \gamma P_2), \quad (66)$$

where

$$\gamma = \frac{f_{L_2}^2}{f_{L_1}^2}. \quad (67)$$

A similar ionospheric-free linear combination for carrier phase may be derived. The carrier phase models can be written as:

$$\begin{aligned} L_1 &= \rho + c(\delta t_R - \delta t^S) + \Delta\rho^{trop} - \Delta\rho_{L_1}^{ion} + \lambda_{L_1} B_{L_1} + \varepsilon, \\ L_2 &= \rho + c(\delta t_R - \delta t^S) + \Delta\rho^{trop} - \Delta\rho_{L_2}^{ion} + \lambda_{L_2} B_{L_2} + \varepsilon, \end{aligned} \quad (68)$$

where λ_{L_1} and λ_{L_2} are the wavelengths at L_1 and L_2 band, and the term λB at each frequency denotes a constant bias expressed in cycles, which contains the integer carrier phase ambiguity N and the phase hardware biases of satellite and receiver. According to Schaer (1999) one cannot separate N from the hardware biases.

Now a linear combination is performed

$$L_{1,2} = n_1 L_1 + n_2 L_2. \quad (69)$$

With similar coefficients as in Eq. 64, the linear combination reads:

$$L_{1,2} = \frac{f_{L_1}^2}{f_{L_1}^2 - f_{L_2}^2} L_1 - \frac{f_{L_2}^2}{f_{L_1}^2 - f_{L_2}^2} L_2 = L_3. \quad (70)$$

The L_3 ionospheric-free linear combination for phase ranges can also be expressed as

$$L_3 = \frac{1}{1 - \gamma} (L_1 - \gamma L_2). \quad (71)$$

4.2.2 Eliminating Higher-Order Ionospheric Effects in GNSS Measurements

The elimination of the ionospheric refraction is the huge advantage of the two ionospheric-free linear combinations Eqs. 66 and 71. Although the term “ionospheric-free” is not completely correct as in this combination the higher-order terms as well as the curvature effects which are less than 0.1 % of the total value in L-band, are neglected.

Based on the geometrical optic approximation Brunner and Gu (1991) proposed an improved model for the ionospheric-free linear combination that considers the significant higher-order terms, the curvature effect of the ray paths, and the effect of the magnetic field. The improved model is written as:

$$L_3 = \frac{1}{1 - \Gamma} (L_1 - \Gamma L_2) - [\kappa_1 - \kappa_2], \quad (72)$$

where κ_1 is the geometric bending effect,

$$\Gamma = \frac{\Gamma_1}{\Gamma_2}, \quad (73)$$

$$\kappa_2 = \frac{\Gamma}{1 - \Gamma} \nu, \quad (74)$$

with the electron collision frequency ν and

$$\Gamma_1 = \frac{C_X}{2f_{L_1}^2} \left(1 \pm \frac{C_Y}{f_{L_1}^2} \overline{N_e B_0 \cos \theta} - \frac{C_X}{4f_{L_1}^2} N_{max} \eta \right), \quad (75)$$

$$\Gamma_2 = \frac{C_X}{2f_{L_2}^2} \left(1 \pm \frac{C_Y}{f_{L_2}^2} \overline{N_e B_0 \cos \theta} - \frac{C_X}{4f_{L_2}^2} N_{max} \eta \right). \quad (76)$$

A comparison of Eq. 71 with Eq. 72 shows that the improved model replaces γ by the more complete Γ and includes two curvature correction terms κ_1 and κ_2 .

4.2.3 Using Multi-Frequency Observations

For this topic we refer to the IERS Conventions 2010 (Petit and Luzum 2010) and references therein.

4.2.4 Very Long Baseline Interferometry and the Ionosphere

Like other space geodetic techniques that operate in the microwave frequency band, Very Long Baseline Interferometry (VLBI) is affected by dispersive delays caused by the ionosphere. Two or more radio telescopes are pointed towards a common radio

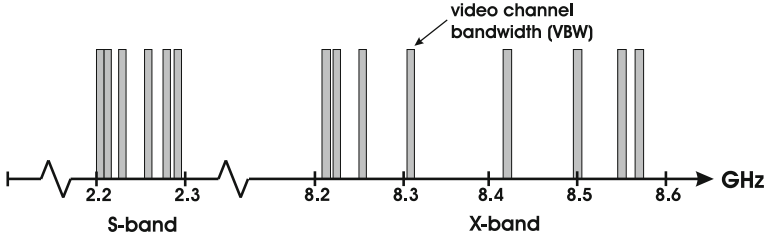


Fig. 2 Typical channel distribution of a geodetic VLBI experiment (the video channel bandwidth is not to scale) (modified from Hobiger (2005))

source which is observed for a certain amount of time in order to cross-correlate the signals. Thereby, so-called fringe phases are the main observables which can be either used for radio astronomical or geodetical purposes. Most of the geodetic experiments are using several video channels per frequency band (see Fig. 2) in order to derive a group delay measurement from the slope of the fringe phases across the covered band.

Thus, other than GNSS which operates with a single carrier, VLBI derived group delays are not assigned to a reference frequency that is actually observed. In a process, called band-width synthesis, phase and group delays are obtained within the so-called fringe fitting procedure by finding the values which maximize the delay resolution function. It can be shown (see e.g. Sekido 2001) that bandwidth synthesis, which takes advantage from Fourier operations, is equivalent to a least squares solution if the correlation amplitude ρ_i of each channel i corresponds to the weight of the phase observable. Thus, one can derive an analytical expression for the so-called effective frequency to which ionosphere group delays can be assigned to. As discussed e.g. in Hobiger (2005) one can express this frequency as

$$f_{gr} = \sqrt{\frac{\sum_{i=1}^N \rho_i \cdot \sum_{i=1}^N \rho_i (f_i - f_0)^2 - \left(\sum_{i=1}^N \rho_i (f_i - f_0) \right)^2}{\sum_{i=1}^N \rho_i (f_i - f_0) \cdot \sum_{i=1}^N \frac{\rho_i}{f_i} - \sum_{i=1}^N \rho_i \cdot \sum_{i=1}^N \rho_i \frac{f_i - f_0}{f_i}}}, \quad (77)$$

where f_0 is a reference sky frequency and f_i is the reference frequency of each channel from which fringe phases are obtained. Equation 77 provide the theoretical basis for the treatment of multi-band delays and their ionospheric contributions in the same way as it would be done for single frequency observations. Instead of the observing frequency the effective ionosphere frequency, computed from the frequency distribution has to be taken to express the ionospheric contribution (measured in TECU) to units of time. The equation reads:

$$\tau_{gr} = \tau_{if} + \frac{\alpha}{f_{gr}^2}, \quad (78)$$

where τ_{gr} and τ_{if} are the observed and ionosphere free group delays. The constituent α is given by

$$\alpha = \frac{40.31}{c} \left(\int N_e ds_1 - \int N_e ds_2 \right) = \frac{40.31}{c} (STEC_1 - STEC_2) . \quad (79)$$

The speed of light c is used for conversion to time delay, s_1 and s_2 are the paths of wave propagation from the source to the first and second station of the radio interferometer. This means that VLBI is only sensitive to differences in the ionospheric conditions. By neglecting higher order ionospheric terms as supported by Hawarey et al. (2005) the linearity of Eq. 78 makes it possible to eliminate ionospheric influences when measurements are carried out at two separated frequency bands.

Ionosphere Free Linear Combination

Nowadays any geodetic VLBI experiment is carried out at two distinct frequency bands in order to correct for ionospheric influences. Taking the standard bands (X- and S-band) for such experiments gives two group delay observable, each of them containing the ionospheric free delay τ_{if} (which will be the input for any precise geodetic analysis) and a contribution α from the ionosphere, scaled by the corresponding effective ionosphere frequencies.

$$\begin{aligned} \tau_{gx} &= \tau_{if} + \frac{\alpha}{f_{gx}^2}, \\ \tau_{gs} &= \tau_{if} + \frac{\alpha}{f_{gs}^2}. \end{aligned} \quad (80)$$

Here the first letter in the indices stands for group or phase delay and the second letter represents X- or S-band. Using these equations the unknown parameter α can be eliminated and the ionospheric free delay observable can be obtained. This is carried out by a simple linear combination between two of the expressions, given in Eq. 80. Considering group delay measurements

$$\tau_{if} = \frac{f_{gx}^2}{f_{gx}^2 - f_{gs}^2} \tau_{gx} - \frac{f_{gs}^2}{f_{gx}^2 - f_{gs}^2} \tau_{gs} . \quad (81)$$

The right part of Eq. 81 can be considered as the observable, from which all geodetic target parameter can be determined. Instead of computing the ionosphere-free linear combination Eq. 81, one can also compute the ionospheric contribution in X-band

$$\tau_{igx} = \frac{\alpha}{f_{gx}^2} = -\frac{f_{gs}^2}{f_{gx}^2 - f_{gs}^2} (\tau_{gx} - \tau_{gs}), \quad (82)$$

add it to the theoretical delay and thus “correct” or “calibrate” the group delay at X-band. This approach should not be applied as the observable would be corrected using the measurement itself. For geodetic analysis the ionosphere-free linear combination should be used, although the ionospheric correction Eq. 82 is usually stored in databases together with all the other information.

Ambiguity Resolution and Ionosphere Delays

Due to the finite number and spacing of the video channels, the delay resolution function is repeating after a certain time lag, which introduces an ambiguity term in the obtained delays. Thereby the ambiguity spacing is equal to the inverse of the greatest common measure of the frequency spacing of the video channels. For most geodetic experiments this spacing is between 50 and 200 ns depending on the selection of the video channels in each band. Although the ambiguity correction is an integer multiple of the basic spacing, it is degraded to a real number when the ionosphere linear combination (Eq. 81) is applied. Moreover, as ambiguity shifts can happen independently in either of the bands, the ionosphere free combination cannot be applied for geodetic estimation purposes until all ambiguity terms have been fixed. This is usually done in an iterative procedure, where the initial ionosphere free linear combination is used in a basic geodetic adjustment for which only clock and troposphere are parameterized. Based on the residuals of this estimation, ambiguity shifts are detected and a new ionosphere free linear combination is formed. Depending on the data quality and the geometry of the VLBI session more than two iterations are necessary to fix all ambiguities. Thereby, delays can be shifted to an arbitrary ambiguity reference, since this constant term will later be absorbed in the station clock offset. Nevertheless, closure conditions need to be taken into account during the ambiguity fixing process, in order not to introduce artificial clock breaks.

Instrumental Biases

In fact, real observations do not exactly correspond to Eq. 80, but rather contain an extra delay term caused by instrumental imperfectness. As mentioned by Ray and Corey (1991) an additional delay is caused by instrumental delays in the different bands, which change the delay observable to

$$\begin{aligned}
 \tau'_{gx} &= \tau_{if} + \frac{\alpha}{f_{gx}^2} + \tau_{inst,x}, \\
 \tau'_{gs} &= \tau_{if} + \frac{\alpha}{f_{gs}^2} + \tau_{inst,s}, \\
 \tau'_{px} &= \tau_{if} - \frac{\alpha}{f_{px}^2} + \tau_{inst,x}, \\
 \tau'_{ps} &= \tau_{if} - \frac{\alpha}{f_{ps}^2} + \tau_{inst,s}.
 \end{aligned} \tag{83}$$

When the ionospheric-free linear combination Eq. 81 is evaluated, a biased delay τ'_{if} is obtained

$$\begin{aligned} \tau'_{if} &= \frac{f_{gx}^2}{f_{gx}^2 - f_{gs}^2} \tau'_{gx} - \frac{f_{gs}^2}{f_{gx}^2 - f_{gs}^2} \tau'_{gs} \\ &= \tau_{if} + \underbrace{\frac{f_{gx}^2}{f_{gx}^2 - f_{gs}^2} \tau_{inst,x} - \frac{f_{gs}^2}{f_{gx}^2 - f_{gs}^2} \tau_{inst,s}}_{\hat{\tau}}, \end{aligned} \tag{84}$$

where the notation $\hat{\tau}$ is used to express overall instrumental delay, caused by a weighted difference between X- and S-band receiving system delays. Although one might think that this would cause a problem in further processing steps, geodetic analysis is not affected by these instrumental delays. As long as instrumental delays do not change between the scans, there will be no impact on geodetic results. They can be treated as a constant bias of the delay measurements, independent of azimuth and zenith distance and are absorbed into the clock models (Ray and Corey 1991). Also the computed ionospheric correction for X-band group delay measurements Eq. 82 has to be replaced now by the intrinsic one ($\tau'_{ig,x}$), including the receiving system biases

$$\begin{aligned} \tau'_{igx} &= -\frac{f_{gs}^2}{f_{gx}^2 - f_{gs}^2} (\tau'_{gx} - \tau'_{gs}) \\ &= \frac{\alpha}{f_{gx}^2} + \underbrace{\frac{f_{gs}^2}{f_{gx}^2 - f_{gs}^2} (\tau_{inst,s} - \tau_{inst,x})}_{\tau_{inst}}. \end{aligned} \tag{85}$$

The scaled difference between S- and X-band instrumental delay, denoted by τ_{inst} , is always contained in the X-band ionospheric correction.

VLBI2010

Since 2003 the International VLBI service for Geodesy and Astronomy (IVS) has been developing the next generation VLBI system called VLBI2010. The VLBI2010 system concept differs from the current geodetic VLBI mode in a variety of ways which also affects the calculations of the ionosphere contribution. With the current data, the geodetic analyst is expected to remove the ionospheric dispersive delay by forming linear combinations and iteratively solving the ambiguity. VLBI2010 will lead to a paradigm change where the dispersive delays are removed during band-width synthesis respectively fringe fitting, taking advantage of the broad-band observables which should permit access to phase delay observables.

4.3 Estimating TEC Using Different Space Geodetic Techniques

Since most of the space geodetic techniques operate in at least two different frequencies, they are capable of eliminating the influence of the ionosphere on the propagation of their signals. This on the other hand provides the ability to gain information about the ionosphere parameters. If the behavior of the ionosphere is known, the ionospheric refraction can be computed and used for development of regional or global models of the ionosphere. Different observation principles result in specific features of the ionosphere parameters derived by each of the techniques. Some of these techniques are:

4.3.1 Determining TEC from GNSS Observations

GNSS including the U.S.A. Global Positioning System (GPS), the Russian Globalnaya Navigatsionnaya Sputnikovaya Sistema (GLONASS), the upcoming European Galileo and the Chinese Beidou system allow for the determination of the station specific ionosphere parameters in terms of STEC values, using carrier phase or code measurements. To extract information about the ionosphere from the GNSS observations, a linear combination is formed, which eliminates the geometric term. This linear combination is called geometry-free linear combination L_4 or the ionospheric observable.

Ionospheric Observable

To form the ionospheric observable, simultaneous observations at two carriers L_1 and L_2 are subtracted. In this way along with the geometric term, all frequency-independent effects such as clock offsets and tropospheric delay are eliminated. This leads to an observable, which contains only the ionospheric refraction and the differential inter-frequency hardware delays. The geometry-free linear combination has the form:

$$L_4 = n_1 L_1 + n_2 L_2 = L_1 - L_2, \quad (86)$$

with $n_1 = 1$ and $n_2 = -1$.

Applying the above combination to the observation equations Eqs. 61 and 68 leads to the geometry-free LC for the code and phase measurements, respectively:

$$P_4 = +\xi_4 I + c \left(\Delta b^S - \Delta b^R \right), \quad (87)$$

$$L_4 = -\xi_4 I + B_4, \quad (88)$$

where:

- $\xi_4 = 1 - f_{L1}^2/f_{L2}^2 \approx -0.647$ factor (GPS) for relating the ionospheric refraction on L_4 to L_1 ,
- $B_4 = \lambda_{L1}B(f_{L1}) - \lambda_{L2}B(f_{L2})$ ambiguity parameter with undefined wavelength, thus defined in length units,
- $\Delta b^S = b^{S,1} - b^{S,2}$ differential inter-frequency hardware delay of the satellite S in time units,
- $\Delta b_R = b_{R,1} - b_{R,2}$ differential inter-frequency hardware delay of the receiver R in time units.

The ionospheric refraction I in Eqs. 87 and 88 can be related to the VTEC as a function of the geomagnetic latitude and the sun-fixed longitude in the following way:

$$I = \xi_E STEC(\beta, s) = \xi_E F(z) VTEC(\beta, s), \tag{89}$$

with:

- $F(z)$ mapping function evaluated at zenith distance z ,
- β geomagnetic latitude,
- s sun-fixed longitude,
- $\xi_E = \frac{c_x}{2} f_1^{-2} \approx 0.162$ m/TECU (GPS).

By substituting Eq. 89 in Eqs. 87 and 88 the ionospheric observable for code and phase measurements reads

$$P_4 \approx +\xi_4 \xi_E F(z) VTEC(\beta, s) + c \left(\Delta b^S - \Delta b_R \right), \tag{90}$$

and

$$L_4 \approx -\xi_4 \xi_E F(z) VTEC(\beta, s) + B_4. \tag{91}$$

In Eqs. 90 and 91, the equation sign ‘=’ has been replaced by the approximate equation sign ‘ \approx ’ because of including the simplified single layer assumption. Depending on the study and whether we want to estimate VTEC on a local, regional or global basis, $VTEC(\beta, s)$ is represented with an appropriate base-function. As an example Taylor series expansion can be used for local representation of TEC; B-splines are very suitable for studying TEC in regional applications, and for global representation of TEC, spherical harmonics expansion is most commonly used. Here we briefly discuss the spherical harmonics expansion approach:

Global TEC Representation Using Spherical Harmonics Expansion

In order to develop a global ionosphere model, the vertical TEC has to be represented as a function of longitude, latitude and time, or according to the definition of the adopted coordinate system given in Sect. 4.3—as a function of the geomagnetic latitude β and sun-fixed longitude s (Schaer 1999):

$$VTEC(\beta, s) = \sum_{n=0}^{n_{max}} \sum_{m=0}^n \tilde{P}_{nm}(\sin \beta) (a_{nm} \cos(ms) + b_{nm} \sin(ms)), \quad (92)$$

where:

- $VTEC(\beta, s)$ vertical TEC in TECU,
- $\tilde{P}_{nm} = N_{nm} P_{nm}$ normalized Legendre function from degree n and order m ,
- N_{nm} normalizing function,
- P_{nm} classical Legendre function,
- a_{nm} and b_{nm} unknown coefficients of the spherical harmonics expansion,

with the normalizing function written as:

$$N_{nm} = \sqrt{\frac{(n-m)!(2n+1)(2-\delta_{0m})}{(n+m)!}}, \quad (93)$$

where δ_{0m} denotes the Kronecker delta. The number of unknown coefficients of spherical harmonics expansion Eq. 92 is given by:

$$u = (n_{max} + 1)^2, \quad (94)$$

and the spatial resolution of a truncated spherical harmonics expansion is given by:

$$\Delta\beta = \frac{2\pi}{n_{max}}, \quad \Delta s = \frac{2\pi}{m_{max}}, \quad (95)$$

where

$\Delta\beta$ is the resolution in latitude, and

Δs is the resolution in sun-fixed longitude and local time, respectively.

It is shown that the mean VTEC (\overline{VTEC}) of the global TEC distribution expressed by Eq. 92 is generally represented by the zero-degree spherical harmonics coefficient \tilde{C}_{00} (Schaer 1999):

$$\overline{VTEC} = \frac{1}{4\pi} \int_0^{2\pi} \int_{-\frac{\pi}{2}}^{+\frac{\pi}{2}} E_v(\beta, s) \cos \beta d\beta ds = N_{00} \tilde{C}_{00} = \tilde{C}_{00}. \quad (96)$$

Parametrization and Estimation of VTEC

To estimate a global VTEC model, GNSS observations from a set of globally distributed GNSS stations are collected. The computation is carried out on a daily basis, using observations with sampling rate of 30 s and elevation cut-off angle 10°. For all of the observations the ionospheric observable is calculated using Eqs. 90 or 91. This observable forms the observation equation. The observation equations are then

solved for every two hour epoch and the unknowns which are the coefficients of the spherical harmonics expansion (a_{nm} and b_{nm} in Eq. 92) are estimated for every two hours (1 h or 15 min solution is also possible) by a least-square adjustment. The estimated unknown coefficients are then entered to calculate grid-wise VTEC values over the globe using Eq. 92. This results in thirteen two-hourly global maps for one complete day. These maps are usually called Global Ionosphere Maps (GIM).

The IONospheric EXchange (IONEX) Format

The GIM are usually provided in the IONospheric EXchange (IONEX) format, described in Schaer et al. (1998). The vertical TEC is represented as a function of geocentric longitude and latitude (λ, β), and time (t) in UT in the form of a raster grid. At the time being, the spatial resolution of this grid is $\Delta\lambda = 5^\circ$ in longitude and $\Delta\beta = 2.5^\circ$ in latitude, and the time resolution of the maps are $\Delta t = 2h$; although the International GNSS Service (IGS) is considering going to higher time resolution of 1 h and finally 15 min.

The interpolation of VTEC for a given epoch T_i with $i = 1, 2, \dots, n$, was proposed by Schaer et al. (1998), which is interpolating between consecutive rotated TEC maps. This can be formulated as follow:

$$VTEC(\beta, \lambda, t) = \frac{T_{i+1} - t}{T_{i+1} - T_i} VTEC_i(\beta, \lambda'_i) + \frac{t - T_i}{T_{i+1} - T_i} VTEC_{i+1}(\beta, \lambda'_{i+1}), \quad (97)$$

with

$$T_i \leq t < T_{i+1} \quad \text{and} \quad \lambda'_i = \lambda + (t - T_i).$$

The TEC maps are rotated by $t - T_i$ around the Z-axis in order to compensate the strong correlation between the ionosphere and the Sun's position. For the grid interpolation, a bi-variate interpolation method can be applied, which uses a simple four-point interpolation formula:

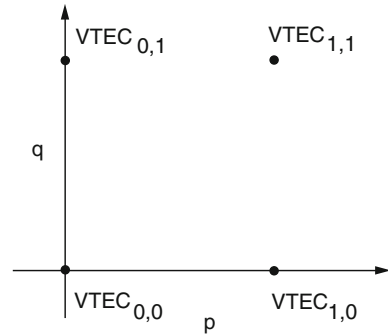
$$VTEC(\lambda_0 + p\Delta\lambda, \beta_0 + q\Delta\beta) = (1 - p)(1 - q)VTEC_{0,0} + p(1 - q)VTEC_{1,0} + (1 - p)qVTEC_{0,1} + pqVTEC_{1,1}, \quad (98)$$

where $0 \leq p < 1$ and $0 \leq q < 1$. $\Delta\lambda$ and $\Delta\beta$ denote the grid widths in longitude and latitude. Figure 3 depicts the interpolation concept.

Ionosphere Working Group of the International GNSS Service

In 1998 a special Ionosphere Working Group (WG) of the IGS was initiated for developing ionospheric products, as described by Schaer et al. (1998) and Hernández-Pajares (2004). The main products provided on a regular basis by the IGS Ionosphere WG are the GIM, representing the VTEC over the entire Earth as a two-dimensional raster in latitude and longitude in two-hourly snapshots, as well as the corresponding

Fig. 3 Bi-variate interpolation using the nearest four TEC values (modified from Schaer et al. 1998)



RMS maps. Additionally, daily and monthly values of the satellite and receiver DCB are provided as well.

The routine generation of ionosphere VTEC maps is currently done at four IGS Associate Analysis Centers (IAAC) for ionosphere products. These IAAC are namely:

- Center for Orbit Determination in Europe (CODE), University of Berne, Switzerland,
- European Space Operations Center of ESA (ESA/ESOC), Darmstadt, Germany,
- Jet Propulsion Laboratory (JPL), Pasadena, U.S.A.,
- Technical University of Catalonia (gAGE/UPC), Barcelona, Spain.

These centers provide results computed with different approaches, which are transmitted to the IGS Ionosphere Product Coordinator, who calculates a weighted combined product. Presently the weights are defined by the IAAC global TEC maps evaluation carried out at the Geodynamics Research Laboratory of the University of the Warmia and Mazury (GRL/UWM) in Olsztyn, Poland (Krankowski et al. 2010). IGS releases a final ionosphere map in IONEX format with resolution of 5° in longitude and 2.5° in latitude with a latency of 10 days and a rapid solution with a latency of 1 day. The IGS GIM and the corresponding RMS maps are available through the IGS server in IONEX format (CDDIS-IONEX 2011).

From long term analysis, it is believed that the IGS VTEC maps have an accuracy of few TECU in areas well covered with GNSS receivers; conversely, in areas with poor coverage, the accuracy can be degraded by a factor of up to five (Feltens et al. 2010).

4.3.2 Obtaining TEC from Satellite Altimetry Measurements

Satellite altimetry is a particular way of ranging in which the vertical distance between a satellite and the surface of the Earth is measured (Seeber 1993). The range between the satellite and the Earth's surface is derived from the traveling time of the radar impulse transmitted by the radar-altimeter and reflected from the ground. Therefore the method is best applicable over the oceans, due to the good reflective properties

of the water. The signals are transmitted permanently in the high frequency domain (about 14 GHz) and the received echo from the sea surface is used for deriving the round-trip time between the satellite and the sea. The satellite-to-ocean range is obtained by multiplication of the traveling time of the electromagnetic waves with the speed of light and averaging the estimates over a second (Todorova 2008).

Satellite Altimetry Missions

The first satellite-borne altimeter missions were the US SKYLAB, consisting of three satellites launched in the period of 1973–1974, GEOS-3 launched in 1975, followed by SEASAT in 1978 and GEOSAT in 1985. As part of several international oceanographic and meteorological programmes a number of satellite altimetry missions were launched in the nineties: ERS-1 (1991–1996), Topex/Poseidon (1992) and ERS-2 (1995). The Jason-1 mission, which was the follow-on to Topex/Poseidon, was launched in 2001 at the same orbit. On the contrary to the ERS-1 and ERS-2 missions, Topex/Poseidon and Jason-1 carried two-frequency altimeters, which gave the opportunity to measure the electron density along the ray path. The latest satellite altimetry mission Jason-2, which is also known as the Ocean Surface Topography Mission (OSTM) was launched in June 2008.

The Topex/Poseidon was a joint project between NASA and the French space agency (CNES) with the objective of observing and understanding the ocean circulation (AVISO 2007). The satellite was equipped with two radar altimeters and precise orbit determination systems, including the DORIS system. The follow-on mission Jason-1 was the first satellite of a series designed to ensure continuous observation of the oceans for several decades. It had received its main features like orbit, instruments, measurement accuracy, and others from its predecessor Topex/Poseidon. The orbit altitude of the two missions was 1,336 km with an inclination of 66° , known as the repeat orbit, causing the satellite pass over the same ground position every 10 days. Jason-1 was followed by Jason-2 as a cooperative mission of CNES, European Organization for the Exploitation of Meteorological Satellites (Eumetsat), NASA, and the National Oceanic and Atmospheric Administration (NOAA). It continued monitoring global ocean circulation, discovering the relation between the oceans and the atmosphere, improving the global climate predictions, and monitoring events such as El Nino conditions and ocean eddies (ILRS 2011). Jason-2 carries nearly the same payload as Jason-1 including the next generation of Poseidon altimeter, the Poseidon-3. The Poseidon-3 altimeter is a two-frequency solid-state sensor, measuring range with accurate ionospheric corrections. Poseidon-3 has the same general characteristics of Poseidon-2, which was onboard Jason-1, but with a lower instrumental noise. The accuracy is expected to be about 1 cm on the altimeter and also on the orbit measurements (Dumont et al. 2009). For more details about the Jason-2 mission refer to CNES (2011).

Ionospheric Parameters from Dual-Frequency Measurements

Although the initial aim of the space-borne altimeters is the accurate measurement of the sea surface height, the two separate operational frequencies give the opportunity to obtain information about TEC along the ray path as well. The primary sensor of both Topex/Poseidon and Jason-1 as well as Jason-2 is the NASA Radar Altimeter, operating at 13.6 GHz (Ku-band) and 5.3 GHz (C-band), simultaneously (Fu et al. 1994). Similar to GNSS, the ionospheric effect on the altimetry measurements is proportional to the TEC along the ray path and inversely proportional to the square of the altimeter frequency. At the Ku-band, the sensitivity of the range delay to the TEC is 2.2 mm/TECU. Thus, the range at this signal can be over-estimated by 2–40 cm due to the ionosphere (Brunini et al. 2005). According to Imel (1994), the precision of the Ku-band range delay correction in one-second data averages is about 5 TECU or 1.1 cm. In fact, the precision of the satellite altimetry derived TEC is a more complex issue, since it is also affected by non-ionospheric systematic effects. A systematic error which might bias the TEC estimates due to its frequency dependence is the so-called Sea State Bias (SSB) (Chelton et al. 2001).

The ionospheric range delay dR derived from the altimeter measurements at the two frequencies is directly provided in mm, and has to be transformed into TECU. It has to be noted, that in the case of satellite altimetry derived TEC no mapping function is needed, since the measurements are carried out normal to the sea surface and thus, the ray path is assumed vertical. Consequently, the transformation formula is:

$$VTEC_{alt} = -dR \cdot 10^{-3} \frac{f_{Ku}^2}{40.31 \cdot 10^{16}} \quad [\text{TECU}], \quad (99)$$

with f_{Ku} being the Ku-band carrier frequency in Hz.

Theoretically, the TEC values obtained by satellite altimetry are expected to be lower than the ones coming from GNSS, since unlike GNSS the altimetry satellites do not sample the topside ionosphere due to their lower orbit altitude. However, several studies have demonstrated that Topex/Poseidon and Jason-1 systematically overestimate the VTEC by about 3–4 TECU compared to the values delivered by GNSS; e.g. Brunini et al. (2005), and Todorova (2008).

4.3.3 Estimating TEC from LEO Satellite Data

Low Earth Orbit (LEO) satellites operate at orbital altitudes between 260 and ~3500 km. Among their different scientific objectives, the global sounding of the vertical layers of the neutral atmosphere and the ionosphere is of great importance. Some of these missions carry dual-frequency GPS receivers onboard, which makes them capable of remote sensing the atmosphere using the Radio Occultation (RO) technique. The RO technique is based on detecting the change in a radio signal passing through the neutral atmosphere and the ionosphere. As a radio signal travels through the atmosphere, it bends depending on the gradient of refractivity normal to

the path. Using the RO measurements onboard a LEO satellite the vertical refractivity profile from the LEO satellite orbit height down to the Earth's surface can be computed. Since the index of refractivity depends mainly on the number of free electrons within the ionosphere, the refractivity profile can be inverted to obtain the vertical Electron Density Profile (EDP) (Jakowski et al. 2002b).

Here we will not go into details about the RO technique and the inversion procedure. For more details about the RO technique refer to e.g. Ware et al. (1996), Rocken et al. (1997), and Jakowski et al. (2004). Details about the inversion procedure could be found in e.g. Schreiner et al. (1999), Hernández-Pajares et al. (2000), and Garcia-Fernandez et al. (2005). In the following some of the LEO missions capable of ionosphere monitoring are briefly described:

The German CHALLENGING Mini-Satellite Payload (CHAMP) was mainly used for geophysical research and application. The satellite was successfully launched by a Russian COSMOS rocket in July 2000. Although the mission was scheduled for five years, providing a sufficient observation time to resolve long-term temporal variations in the magnetic field, the gravity field and within the atmosphere, the mission lasted more than ten years and the satellite re-entered the Earth's atmosphere on September 2010. The advanced "Black Jack" GPS receiver developed by the JPL could measure GPS carrier phases in the limb sounding mode, starting at CHAMP orbit tangential heights down to the Earth's surface (Jakowski et al. 2002a). The RO measurements performed on board CHAMP were used to retrieve vertical temperature profiles of the global troposphere/stratosphere system (Wickert et al. 2001). The first ionospheric radio occultation (IRO) measurements were carried out in April 2001 yielding reasonable electron density profiles (Jakowski et al. 2002b).

The Gravity Recovery and Climate Experiment (GRACE) is a NASA and German Aerospace Center (DLR) science mission satellite system, established to measure primarily variations in the Earth's gravity field. The system consists of two satellites in a near-polar orbit at about 500km altitude in the same orbital plane 220km apart. The twin satellites were launched in March 2002 with an expected life of five years; however the satellites are still operating by the end of 2012. The dual-frequency Blackjack GPS receivers were used for precise orbit determination and atmospheric occultation on each of the satellites, providing capability of global monitoring of the vertical electron density distribution (Wickert et al. 2005).

The Formosat-3/COSMIC-Formosa Satellite Mission-Constellation Observing System for Meteorology, Ionosphere and Climate (F3C) is a joint project between Taiwan and the U.S.A. for weather, climate, space weather, and geodetic research. The F3C mission was successfully launched in April 2006. The mission consists of six micro satellites, each carrying an advanced GPS RO receiver, a Tiny Ionospheric Photometer (TIP) and a Tri Band Beacon (TBB) (Rocken et al. 2000). The satellites were gradually raised from their launched orbit to reach their final orbit altitude of 800km. F3C mission is currently providing between 1000 and 2500 daily RO profiles in the neutral atmosphere, 1000 and 2500 daily electron density profiles and total electron content arcs, and TIP radiance products (COSMIC 2011).

4.3.4 Determining Ionospheric Parameters from VLBI Data

Although VLBI is a differential space geodetic technique it is possible to derive absolute ionosphere parameters, i.e. VTEC for each station. As shown by Hobiger et al. (2006) VTEC values can be determined similar as troposphere parameters (see section on mapping functions and gradients by Nilsson et al. (2013) in this book) by taking advantage of the fact that the slant ionosphere delays are elevation dependent and can be described by an empirical mapping function (Eq. 50). Thus VTEC values can be estimated for each station and constant instrumental delays can be separated from these parameters within the adjustment process. As one of the drawbacks, the estimation of ionosphere parameters from VLBI needs a mathematical relation between VTEC above the site and the VTEC of each observation as described in Hobiger (2005) or Hobiger et al. (2006). Moreover, as VLBI provides only a single scan per epoch and station, it is important that mapping function errors are reduced to a minimum in order to obtain unbiased VTEC estimates. Dettmering et al. (2011a) carried out a thorough investigation of systematic differences between VTEC obtained by different space-geodetic techniques including VLBI by applying the estimation strategy proposed by Hobiger et al. (2006). Thereby it is concluded that VLBI derived ionosphere parameters are comparable to other space geodetic techniques, like GPS, DORIS, Jason and F3C concerning the accuracy of the estimation. Moreover, the mean biases found in that study are similar to those given in Hobiger et al. (2006) being in the range of a few TECU.

4.3.5 Acquiring Ionospheric Information from DORIS

The Doppler Orbitography and Radio positioning Integrated by Satellite (DORIS) was developed by the French CNES, Institut Géographique National (IGN) and Groupe de Recherche en Géodésie Spatiale (GRGS) to meet scientific and operational user requirements in very precise orbit determination. Although the DORIS system was primarily designed for the precise orbit computation required for observing the oceans by altimetry missions, the unique network of ground stations and its highly accurate positioning capability have also played a great role for geodesy and geophysical applications. This includes measuring continental drift, fitting the local geodetic network, monitoring the geophysical deformations, determining the rotation and the gravity parameters of the Earth, and contributing to the realization of an international terrestrial reference system. Due to the fact that the DORIS system uses two different frequencies for its measurement, it is capable of monitoring the ionosphere as well.

The basic principle of the DORIS system is based on the accurate measurement on board the spacecraft of the Doppler shift of radio frequency signals emitted by ground beacons. Measurements are made on two frequencies: ~ 2 GHz and 400 MHz. About 56 ground beacon stations transmit dual frequency signals from locations distributed all over the world. The satellites carrying the DORIS receivers include Jason, TOPEX, ENVISAT, SPOT 2, SPOT 4, and SPOT 5. These satellites are at the

range of 800–1,336 km altitude. The ionospheric products deduced from the Doppler measurements are recorded at each count interval of about 10 s, and are used to derive the ionospheric TEC. The ionospheric corrections are available at the CDDIS website (CDDIS 2011). For more details on DORIS mission refer to Fleury et al. (1991) or Yin and Mitchell (2011).

4.3.6 Combination of Different Techniques

Although each of the above mentioned techniques is capable of providing information about the ionosphere, each technique has its pros and cons depending on its characteristics. The classical input data for development of GIM are obtained from dual-frequency observations carried out at GNSS stations. However, GNSS stations are in-homogeneously distributed around the world, with large gaps particularly over the oceans; this fact reduces the precision of the GIM over these areas. On the other hand, dual-frequency satellite altimetry missions such as Jason-1 (see Sect. 4.3.2) provide information about the ionosphere precisely above the oceans; and furthermore LEO satellites, such as F3C (see Sect. 4.3.3) provide well-distributed information of ionosphere on globe. Combining different techniques for developing the ionospheric maps would significantly improve the accuracy and reliability of the developed model, as the combined model uses the advantages of each particular method and provides a more accurate result than from each single techniques alone.

Several studies have investigated the development of combined models of the ionosphere. Todorova et al. (2007) developed combined models of VTEC from GNSS and satellite altimetry data. Alizadeh et al. (2011) developed models using combination of GNSS, satellite altimetry and F3C measurements. Both studies aimed at

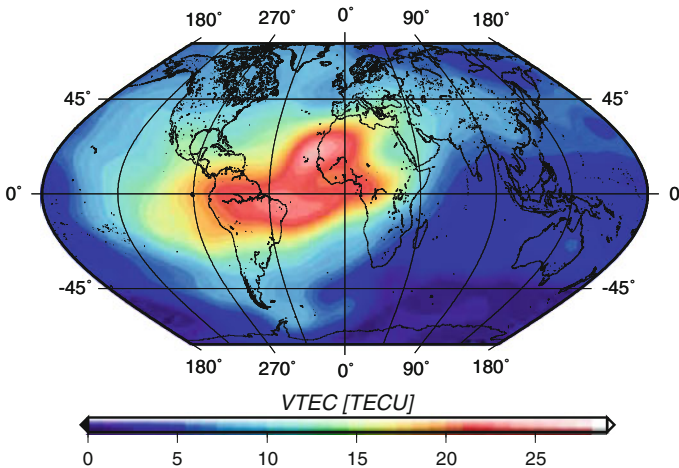


Fig. 4 GNSS, satellite altimetry, and F3C combined GIM, 17UT, day 202, 2007 (Alizadeh et al. 2011)

developing combined maps globally. Dettmering et al. (2011b) performed combination of different techniques for regional modeling of the ionosphere. All these studies prove that the combined maps provide a more homogeneous coverage and higher accuracy and reliability than results of each single method. Figure 4 depicts a snapshot of a GNSS, satellite altimetry, and F3C combined GIM at 9UT of day 202, 2007 (Alizadeh et al. 2011).

Acknowledgments The authors wish to express their heartfelt gratitude to Manuel Hernández-Pajares from the Research group of Astronomy and GEomatics (gAGE) of the Technical University of Catalonia (UPC)—Barcelona, and also to Michael Schmidt from the Deutsches Geodätisches Forschungsinstitut (DGFI)—Munich, for the revision of this part and their valuable advice for improving the script. The Austrian Science Fund (FWF Der Wissenschaftsfonds) is also deeply appreciated for funding projects VlbIonos (project P16136), COMBION (project P19564), MDION (project P22203), and GGOS Atmosphere (project P20902).

References

- M.M. Alizadeh, H. Schuh, S. Todorova, and M. Schmidt. Global ionosphere maps of VTEC from gnss, satellite altimetry, and Formosat-3/COSMIC data. *J. Geod.*, 85 (12): 975–987, December 2011.
- AVISO. The French active archive data center for multi-satellite altimeter missions, 2007. <http://www.aviso.oceanobs.com>.
- S. Bassiri and G.A. Hajj. Higher-order ionospheric effects on the global positioning system observables and means of modeling them. *Manuscripta Geodaetica*, 18: 280–289, 1993.
- M. Bauer. *Vermessung und Ortung mit Satelliten - GPS und andere satellitengestützte Navigationssysteme*. Wichmann, Karlsruhe, 5th Edition, 2003.
- D. Bilitza, L.A. McKinnell, B. Reinisch, and T. Fuller-Rowell. The International Reference Ionosphere today and in the future. *J. Geod.*, 85: 909–920, December 2011.
- D. Bilitza and B.W. Reinisch. International Reference Ionosphere 2007: Improvements and new parameters. *Adv. Space Res.*, 42: 599–609, 2007.
- J. Böhm, D. Salstein, M. Alizadeh, and D. D. Wijaya. Geodetic and atmospheric background. In J. Böhm and H. Schuh, editors, *Atmospheric Effects in Space Geodesy*. Springer-Verlag, 2013.
- M. Born and E. Wolf. *Principles of optics: electromagnetic theory of propagation, interference and diffraction of light*. Macmillan, New York, 2nd Edition, 1964.
- C. Brunini, A. Meza, and W. Bosch. Temporal and spatial variability of the bias between TOPEX- and GPS-derived total electron content. *J. Geod.*, 79 (4–5):175–188, 2005.
- F.K. Brunner and M. Gu. An improved model for the dual frequency ionospheric correction of GPS observations. *Manuscripta geodaetica*, 16(3):205–214, 1991.
- K.G. Budden. *The propagation of radio waves*. Cambridge Univ. Press, 1985.
- CDDIS. CDDIS ftp site. Website, 2011. <ftp://cddis.gsfc.nasa.gov/>.
- CDDIS-IONEX. IONEX ftp site. Website, 2011. <ftp://cddis.gsfc.nasa.gov/pub/gps/products/ionex>.
- D.B. Chelton, J.C. Ries, B.J. Haines, L.L. Fu, and P. Callahan. *Satellite altimetry and Earth sciences: A handbook of techniques and applications*. Academic Press, London, 2001.
- CNES. Jason-2 altimetry mission for ocean observation, 2011. <http://smc.cnes.fr/JASON2/index.htm>.
- COSMIC. Cosmic program official. Website, 2011. <http://www.cosmic.ucar.edu/about.html>.
- R. Dach, U. Hugentobler, P. Fridez, and M. Meindl. *Bernese GPS Software*, Version 5.0. Astronomical Institute, University of Bern, 2007.

- D. Dettmering, R. Heinkelmann, M. Schmidt. Systematic differences between VTEC obtained by different space-geodetic techniques during CONT08. *J. Geod.*, 85:443–451, 2011a.
- D. Dettmering, M. Schmidt, R. Heinkelmann, and M. Seitz. Combination of different space-geodetic observations for regional ionosphere modeling. *J. Geod.*, 85: 989–998, 2011b.
- G. Di Giovanni and S.M. Radicella. An analytical model of the electron density profile in the ionosphere. *Adv. Space Res.*, 10 (11): 27–30, 1990.
- J.P. Dumont, V. Rosmorduc, N. Picot, S. Desai, H. Bonekamp, J. Figa, J. Lillibridge, and R. Scharroo. *OSTM/Jason-2 Products Handbook*. CNES and EUMETSAT and JPL and NOAA/NESDIS, 4th Edition, August 2009.
- J. Felten, M. Angling, N. Jackson-Booth, N. Jakowski, M. Hoque, C. Mayer, M. Hernández-Pajares, A. García-Rigo, R. Orús-Perez, A. Aragón-Angel, and M.J. Zornoza. GNSS contribution to next generation global ionospheric monitoring. Technical report, ESA/ESOC Final Report, January 2010.
- R. Fleury, F. Foucher, and P. Lassudrie-Duchesne. Global TEC measurements capabilities of the DORIS system. *Adv. Space Res.*, 11 (10): 1051–1054, 1991.
- M. Fritsche, R. Dietrich, C. Knöfel, A. Rülke, and S. Vey. Impact of higher-order ionospheric terms on GPS estimates. *Geophys. Res. Lett.*, 32, L23311, 2005
- L.L. Fu, E.J. Christensen, C.A. Yamarone, M. Lefebvre, Y. Ménard, M. Dorner, and P. Escudier. Topex/Poseidon mission overview. *J. Geophys. Res.*, 99 (C12):24369–24382, 1994.
- M. García-Fernandez, M. Hernández-Pajares, J.M. Juan, and J. Sanz. Performance of the improved Abel transform to estimate electron density profiles from GPS occultation data. *GPS Solut*, 9: 105–110, 2005.
- G. K. Hartmann and R. Leitinger. Range errors due to ionospheric and tropospheric effects for signal frequencies above 100 MHz. *Bull. Géod.*, 58: 109–399, 1984.
- M. Hawarey, T. Hobiger, and H. Schuh. Effects of the 2nd order ionospheric terms on VLBI measurements. *Geophys. Res. Lett.*, 32, L11304, 2005.
- M. Hernández-Pajares. IGS Ionosphere WG Status Report: Performance of IGS Ionosphere TEC map. Technical report, IGS Workshop, Bern, Switzerland, 2004.
- M. Hernández-Pajares, J.M. Juan, and J. Sanz. Improving the Abel inversion by adding ground GPS data to LEO radio occultation in ionospheric sounding. *Geophys. Res. Lett.*, 27 (16): 2473–2476, 2000.
- M. Hernández-Pajares, J.M. Juan, J. Sanz, and D. Bilitza. Combining GPS measurements and IRI model values for space weather specification. *Adv. Space Res.*, 29 (6): 949–958, 2002.
- T. Hobiger. *VLBI as tool to probe the ionosphere*. PhD thesis, Inst. of Geodesy and Geophysics, Vienna Univ. of Technology, Austria, 2005.
- T. Hobiger, T. Kondo, H. Schuh. Very long baseline interferometry as a tool to probe the ionosphere. *Radio Science*, 41 (1): RS1006, 2006.
- B. Hofmann-Wellenhof, H. Lichtenegger, and J. Collins. *GPS Theory and Practice*. Springer, Wien New York, 2nd Edition, 1993.
- ILRS. Jason2 satellite information. Website, 2011. http://ilrs.gsfc.nasa.gov/satellite_missions/list_of_satellites/jas2_general.html.
- D.A. Imel. Evaluation of the TOPEX/POSEIDON dual-frequency ionosphere correction. *J. Geophys. Res.*, 99 (12): 24895–24906, 1994.
- ITU. ITU-R Recommendation, 2007. <http://www.itu.int/ITU-R>.
- ITU. Radiocommunication sector. Website, 2011. <http://www.itu.int/oth/R0A04000018/en>.
- N. Jakowski, R. Leitinger, and M. Angling. Radio occultation techniques for probing the ionosphere. *Annals of Geophysics*, Supplement to Vol. 47: 1049–1066, 2004.
- N. Jakowski, A. Wehrenpfennig, S. Heise, C. Reigber, and H. Lühr. Status of ionospheric radio occultation CHAMP data analysis and validation of higher level data products. In *1st CHAMP Science Meeting*, Potsdam - Germany, 22–25 January 2002a.
- N. Jakowski, A. Wehrenpfennig, S. Heise, CH. Reigber, H. Lühr, L. Grunwaldt, and T. Meehan. GPS radio occultation measurements of the ionosphere from CHAMP early results. *Geophys. Res. Lett.*, 29 (10), 2002b.

- JPL. JPL - NASA, Gaim introduction. Website, 2011. <http://iono.jpl.nasa.gov/gaim/intro.html>.
- J. Klobuchar. Design and characteristics of the GPS ionospheric time-delay algorithm for single-frequency users. In *PLANS'86 - Position Location and Navigation Symposium*, pages 280–286, Las Vegas, Nevada, 4–7 November 1986.
- J. A. Klobuchar. *Ionospheric effects on GPS, in Global Positioning System: Theory and Application*, Volume I. American Institute of Aeronautics and Astronautics, Washington DC., 1996.
- A. Krankowski, M. Hernandez-Pajares, J. Feltens, A. Komjathy, S. Schaer, A. Garcia-Rigo, and P. Wielgosz. Present and future of IGS ionospheric products. Technical report, IGS Workshop, Newcastle, England, 2010.
- L.K. Lilov. On stabilization of steady-state motions of mechanical systems with respect to a part of the variables. *Journal of Applied Mathematics and Mechanics*, 36(6):922–930, 1972.
- M. Materassi. Ionospheric Tomography, 3d and 4d imaging and data assimilation. In *invited paper*, Matera, Italy, 13–15 October 2003. Atmospheric Remote Sensing using Satellite Navigation Systems Special Symposium of the URSI Joint Working Group FG, ASI Centro di Geodesia Spaziale 'Giuseppe Colombo'.
- C.N. Mitchell and P.S. Cannon. Multi-instrumental data analysis system (MIDAS) imaging of the ionosphere. Technical report, University of Bath, United States Air Force European Office of Aerospace Research and Development, February 2002.
- C.N. Mitchell and P.S.J. Spencer. A three dimensional time-dependent algorithm for ionospheric imaging using GPS. *Annal. Geophysics*, 46 (4): 687–696, 2003.
- M. Mosert de Gonzalez and S.M. Radicella. On a characteristic point at the base of the F2 layer in the ionosphere. *Adv. Space Res.*, 10 (11):17–25, 1990.
- B. Nava. A near real-time model-assisted ionosphere electron density retrieval method. *Radio Science*, 41(6), 2006.
- B. Nava, P. Coisson, and S.M. Radicella. A new version of the Nequick ionosphere electron density model. *J. Atmos. Solar-Terr. Phys.*, 70: 1856–1862, 2008.
- T. Nilsson, J. Böhm, D. D. Wijaya, A. Tresch, V. Nafisi, and H. Schuh. Path delays in the neutral atmosphere. In J. Böhm and H. Schuh, editors, *Atmospheric effects in space geodesy*. Springer-Verlag, 2013. this book.
- U.S. Naval Research Laboratory Press Release NRL. Updated version of GAIM model goes operational. Website, 2008. <http://www.nrl.navy.mil/pao/pressRelease.php?Y=2008&R=30-08r>.
- R. Orús, M. Hernández-Pajares, J.M. Juan, J. Sanz, and M. García-Fernández. Performance of different TEC models to provide GPS ionospheric corrections. *J. Atmos. Solar-Terr. Phys.*, 64 (18): 2055–2062, 2002.
- G. Petit and B. Luzum, editors. IERS Conventions 2010. Technical Report 36, 2010.
- S.M. Radicella. The Nequick model genesis, uses and evolution. *Annals of Geophysics*, 52 (3/4): 417–422, 2009.
- S.M. Radicella and R. Leitinger. The evolution of the DGR approach to model electron density profiles. *Adv. Space Res.*, 27 (1): 35–40, 2001.
- S.M. Radicella and B. Nava. Nequick model: Origin and evolution. In *Antennas Propagation and EM Theory (ISAPE)*, pages 422–425. IEE Xplore, November - December 2010.
- J.R. Ray and B.E. Corey. Current precision of VLBI multi-band delay observables. In *Proceedings AGU Chapman Conference on Geodetic VLBI: Monitoring Global Change*, Washington D.C., 22–26 April, 1991.
- C. Rocken, R. Anthes, S. Sokolovskiy, M. Exnerand, D. Hunt, R. Ware, M. Gorbunov, W. Schreiner, D. Feng, B. Herman, Y. Kuo, and X. Zou. Analysis and validation of GPS/MET data in the neutral atmosphere. *J. Geophys. Res.*, 102: 29849–29866, 1997.
- C. Rocken, Y.H. Kuo, W. Schreiner, D. Hunt, and S. Sokolovskiy. Cosmic system description. *Atmospheric and Oceanic Science*, 11 (1): 21–52, March 2000.
- S. Schaer. *Mapping and predicting the Earth's ionosphere using the Global Positioning System*. PhD thesis, Bern University, Switzerland, 1999.

- S. Schaer, W. Gunter, and J. Felten. Ionex: The ionosphere map exchange format version 1. In *J. M. Dow, J. Kouba, and T. Springer (Eds.), pages 233–247, Darmstadt, Germany, 1998. Proceeding of the IGS AC Workshop.*
- L. Scherliess, R.W. Schunk, J.J. Sojka, and D.C. Thompson. Development of a physics-based reduced state Kalman filter for the ionosphere. *Radio Sci.*, 39, 2004.
- W. Schreiner, S. Sokolovskiy, C. Rocken, and D. Hunt. Analysis and validation of GPS/MET radio occultation data in the ionosphere. *Radio Sci.*, 34 (4): 949–966, 1999.
- G. Seeber. *Satellite Geodesy, Foundations, Methods and Application*. Walter de Gruyter, Berlin, New York, 1993.
- M. Sekido. *Pulsar Astrometry by VLBI*. PhD thesis, Department of Astronomical Science, School of Mathematical and Physical Science, The Graduate University for Advanced Studies, Mitaka, Tokyo, Japan, 2001.
- L. Sirovich and R. Everson. Management and analysis of large scientific datasets. *Int. J. Supercomputer Appl.*, 6: 50–68, 1992.
- L. Sparks, Lijima B.A., Mannucci A.J., Pi X., and Wilson B.D. A new model for retrieving slant TEC corrections for wide area differential GPS. In *2000: Navigating into the New Millennium*, pages 464–473, Anaheim, CA; United States, 26–28 Jan. 2000. Institute of Navigation National Technical Meeting.
- S. Todorova. *Combination of space geodetic techniques for global mapping of the ionosphere*. PhD thesis, Vienna University of Technology, Austria, 2008.
- S. Todorova, H. Schuh, and T. Hobiger. Using the global navigation satellite systems and satellite altimetry for combined global ionosphere maps. *Adv. Space Res.*, 42: 727–736, 2007.
- A.J. Tucker and B.M. Fanin. Analysis of ionospheric contributions to the Doppler shift of CW signals from artificial satellites. *J. Geophys. Res.*, 73: 4325–4334, 1968.
- R. Ware, D. Exner, M. Feng, K. Gorbunov, K. Hardy, B. Herman, Y. Kuo, T. Meehan, W. Melbourne, C. Roken, W. Schreiner, S. Sokolovskiy, F. Solheim, X. Zou, R. Anthes, S. Businger, and K. Trenberth. GPS sounding of the atmosphere from low earth orbit: preliminary results. *Bull. Am. Meteor. Soc.*, 77: 19–40, 1996.
- D.E. Wells. Doppler satellite control. Technical Report 29, UNB, Fredricton, 1974.
- J. Wickert, G. Beyerle, R. König, S. Heise, L. Grunwaldt, G. Michalak, C. Reigber, and T. Schmidt. GPS radio occultation with CHAMP and GRACE: A first look at a new and promising satellite configuration for global atmospheric sounding. *Annales Geophysicae*, 23 (3): 653–658, 2005.
- J. Wickert, Ch. Reigber, G. Beyerle, R. König, Ch. Marquardt, T. Schmidt, L. Grunwaldt, R. Galas, T. Meehan, WG. Melbourne, and K. Hocke. Atmosphere sounding by GPS radio occultation: First results from CHAMP. *Geophys. Res. Lett.*, 28: 3263–3266, 2001.
- P. Yin and C. N. Mitchell. Demonstration of the use of the doppler orbitography and radio positioning integrated by satellite (DORIS) measurements to validate GPS ionospheric imaging. *Adv. Space Res.*, 48: 500–506, 2011.